論文 / 著書情報
Article / Book Information

Title	The development of B/Cr co-doped DLC coating by FCVA deposition system and its tribological properties at 300°C
Authors	Ruixi Zhang, Woo-Young Lee, Noritsugu Umehara, Takayuki Tokoroyama, Motoyuki Murashima, Yuji Takimoto
Citation	Surface & Coatings Technology, Vol. 487, No. 130968, pp. 1-10
Pub. date	2024, 7
DOI	https://dx.doi.org/10.1016/j.surfcoat.2024.130968
Creative Commons	Information is in the article.

Surface & Coatings Technology 487 (2024) 130968

Contents lists available at ScienceDirect

Surface & Coatings Technology

journal homepage: www.elsevier.com/locate/surfcoat

The development of B/Cr co-doped DLC coating by FCVA deposition system and its tribological properties at 300 °C

Ruixi Zhang [a,*], Woo-Young Lee [a,b], Noritsugu Umehara [a], Takayuki Tokoroyama [a], Motoyuki Murashima [a,c], Yuji Takimoto [d]

[a] Department of Micro-nano Mechanical Science and Engineering, Nagoya University, Japan
[b] Intelligent Optical Module Research Center, Korea Photonics Technology Institute, Republic of Korea
[c] Department of Mechanical Systems Engineering, Tohoku University, Japan
[d] Toyo Tanso Co., Ltd., Japan

ARTICLE INFO

Keywords:
DLC coating
FCVA
High temperature tribological properties
Argon gas assisted arc deposition
Boron/chromium co-dopants

ABSTRACT

The diamond-like carbon (DLC) coating prepared using filtered cathodic arc deposition (FCVA) lost its promising wear resistance under high temperatures. Element-doped DLC coatings have been investigated to suppress carbon oxidation reaction and subsequently enhance the wear resistance in high-temperature environments. Previous research clarified the excellent tribological properties of boron-doped DLC (B-DLC) but identified challenge such as arc discharge extinguishment and coating declamation (under high-temperature friction test). In this study, the introduction of Argon gas (10 sccm) during the deposition process stabilized stable arc discharge, resulting in high hardness and deposition rate. Moreover, a chromium interlayer and varying concentration of Cr dopant (0.5 %, 1.0 %, 3.0 % at.) were added to B-DLC to develop a stable, co-doped DLC with low friction and high wear resistance. Raman spectroscopy and nano-indentation revealed an increase in the disordered carbon structure and reduction in hardness and Young's Modulus with Cr doping. Macroscopic ball-on-disk friction test, showed 1 % Cr-doped B-DLC (a-C:B:Cr_1) coating exhibited super low friction (avg. coefficient 0.02) and a low specific wear rate ($<5.0 \times 10^{-6}$ mm^3/Nm). Raman spectroscopy indicated that the transferred graphite-like tribo-film onto the surface of Si_3N_4 counterparts contributed to stable low friction. Additionally, XPS analysis on the DLC coatings' wear track suggested the rich B—B bond might contribute to its high wear resistance. This successful improvement on element-doped DLC prepared by FCVA provided valuable insights for further exploration of DLC coating applied to various working situations.

1. Introduction

Diamond-like Carbon (DLC), with high hardness and chemical inertness, is one of the most common amorphous carbon materials, featuring a combination of sp^2 and sp^3 hybridized carbon atoms. Its novel tribological properties, along with corrosion resistance, have expanded the extensive exploration in various research fields, such as, biomedical [1–5], material science [6–9], and optical fields [2,10,11]. In particular, due to its significant structure, DLC coating can realize low friction and exhibit high wear resistance, serving as an outstanding solid lubricant to protect the friction counterparts [12–14]. In sight of global warming issues and urgent need to reduce carbon emission, the typical tribological properties of DLC coatings may improve energy efficiency and reduce gas emission compared with conventional lubricant material [15]. Therefore, DLC coatings have garnered significant attention for applications in automobile and manufacturing industries. There has been a notable increase in DLC-related research, including the preparation method [16–21], structural characterization [22–27], evaluation on mechanical and tribological properties [28–30] and so on [31]. Various types of deposition methods have been further developed in the past decades [32–34]. Filtered cathodic vacuum arc (FCVA) deposition system has become widely used to prepare defect-free DLC coating with high hardness and promising wear resistance [35–39]. The so-called tetrahedral amorphous carbon (ta-C) coating deposited by FCVA devices, containing >60 % sp^3 structure and usually exhibiting the hardness higher than 40 GPa, were further investigated as the considerable alternative materials of conventional DLC coatings and applied to various frictional counterparts and lubrication situations [40].

* Corresponding author.
E-mail address: ruixi.zhang@mae.nagoya-u.ac.jp (R. Zhang).

https://doi.org/10.1016/j.surfcoat.2024.130968
Received 13 February 2024; Received in revised form 29 May 2024; Accepted 30 May 2024
Available online 12 June 2024

Around two decades ago, the academic interest and challenge related to DLC coating on tribological properties shifted towards the application in high temperature atmosphere and other ultra-harsh environments [41–47]; Deng et al. [48] found that ta-C coating still maintained a low friction coefficient ($\mu < 0.1$) in air even when the environmental temperature exceeded 500 °C. However, the coating was dramatically worn out once the temperature reached over 200 °C. Consequently, it has been reported that the elements doped into DLC coatings, for instance, boron (B), silicon (Si), [49] chromium (Cr), [50] tungsten (W) [51] can suppress the oxidation reaction of carbonaceous coating, thereby improving the thermal resistance and the wear resistance at elevated high temperature. For instance, Hofmann et al. [49] prepared three types of Si-doped DLC with various dopant concentrations, revealing the indentation hardness and friction coefficient remained stable as the environment temperature increased to 500 °C. Furthermore, W-doped DLC [51] was found to exhibit low friction and low wear under high temperature of 400 °C and 500 °C, where tungsten trioxide (WO_3) richly detected in the transfer layer was interpreted as the main factor of superior tribological properties above-mentioned.

In our previous research, we found the boron doped DLC (B-DLC) deposited by FCVA can maintain low friction coefficient and exhibit high wear resistance at 300 °C [52]; the graphitization transfer layer promoted by high temperature are the main factor of low friction, and the incorporation of boron dopant suppress the oxidation of carbonaceous coating, resulting in the high wear resistance of DLC coating. However, we also observed issues such as the extinguishment of arc discharge during deposition process, as well as the easy delamination of coatings, significantly restricting the practical application of DLC coating. In details, arc discharge occurred on the carbon target surface, subsequently generating carbon plasma. However, when using a boron dopant-included target arc frequently extinguished, causing the coating process to cease and adversely affecting both the quality and productivity of the coating. In addition, delamination consistently occurred due to the weakening adhesion force between the coating and substrate during friction, resulting in high friction and severe wear. Therefore, our objective was to address these two issues to unlock the potential for a long-term, hard carbonaceous coating with exceptionally low friction and wear. Building on insight from this previous research, we started with the development of coating design, as well as FCVA deposition characteristic to make progress towards this high-temperature friendly B-DLC.

In this research, we designed to introduce the Cr interlayer to buffer the hardness difference between soft substrate and hard DLC coating, enhancing the adhesion force and protecting the delamination of DLC coating from substrate under high-temperature friction test [53]. Furthermore, while tackling the challenge of extinguishment during the coating procedure, we identified a crucial factor: the internal pressure of the vacuum chamber significantly influenced the extinguishment, a phenomenon we diligently monitored throughout the process. To counter this, we proposed the introduction of Argon gas to enhance electron atom presence, thereby ensuring the continuity of arc discharge. This concept was inspired by the stabilizing effect of Argon gas on plasma generation during the sputtering process [54,55]. In this study we focused on developing the deposition continuity of FCVA system, optimizing deposition parameters and discussing the mechanism of Argon gas effect on the DLC preparation [24]. Moreover, DLC coatings modified by co-dopant elements (B/Cr) began to be explored to achieve synthetic effects [56,57], in details, Cr-DLC was reported to maintain low friction and high wear resistance at high temperature [58,59]; besides, the Cr-incorporated DLC will exhibit affinity with Cr interlayer. Thus, we proposed to prepare the thermal stable a-C:B:Cr coating exhibiting superior tribological properties at 300 °C in air.

We employed the structural characterization, evaluating the mechanical properties by nano-indentation and profilometer. In addition, the macro ball-on disk friction tests were conducted at 300 °C, figuring out the tribological properties of a-C:B:Cr coatings and identifying the optimal concentration of chromium dopant. Finally, electron microscopy, Raman spectroscopy, X-ray Photoelectron Spectroscopy (XPS) were used to clarify the friction and wear mechanism of a-C:B:Cr coatings, and reveal the influence of embedded co-dopants on coating design and tribological properties.

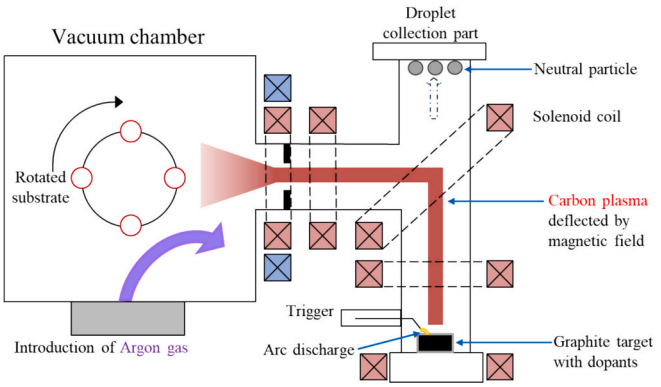

Fig. 1. Schematic diagram of T-shaped FCVA deposition system, where carbon plasma with the dopant-induced plasma (B/Cr) was generated by arc discharge, bending 90° under the magnetic force and finally depositing on the rotated cathodic substrate. Neutral particles and impurities mixed in the original carbon target were gathered in the frontal collection area. In addition, Argon gas was introduced, then ionized at the arc discharge area, providing sufficient electron for the continuous arc discharge of carbon plasma.

2. Experimental

2.1. Coating preparation

The a-C:B:Cr coating was prepared on an Inconel disk and deposited by the T-shaped filtered cathodic vacuum arc (FCVA) deposition system, as illustrated in Fig. 1 [60,61]. A Cr film was served as an interlayer to strengthen the adhesion between Inconel substrate and a-C:B:Cr coating. The Inconel disk (with the size of 20 mm in diameter and 2 mm in thickness), was composed of nickel (68 %), chromium (17 %) and iron (8 %), and selected as the substrate due to its high strength and thermal stability under high temperature. The Cr interlayer with the thickness of 50 nm, was fabricated by magnetron sputter prior to main DLC deposition. The T-shaped FCVA equipment utilized magnetic force and can remove the neutral atoms and macro-particles by employing a 90° curved filter. Prior to the main deposition, the surface of all samples was ultrasonically cleaned with acetone and alcohol for 15 mins each. The cylindrical graphite target (with 50 mm in diameter and 24 mm in height), incorporated in boron (5.0 at. %) as well as Cr dopants (0.5, 1.0, 3.0 at. %) (provided by Toyo Tanso Co., Ltd.) was used as the carbon source of DLC films. In this study, we labeled the coating using a consistent Cr-dopant atomic concentration; for example, a-C:B:$Cr_{0.5}$ corresponded to the coating deposited with a 0.5 % Cr dopant included in the graphite target. The deposition was carried out by following the three steps, reported in our previous works [60,61]: (1) pre arc on the graphite target, (2) Argon-plasma etching and (3) a-C:B:Cr coating deposition. The chamber was initially vacuumed below 4.0×10^{-3} Pa, and the work pressure mainly fluctuated around the 0.02 Pa during the

Table 1
Conditions for a-C:B:Cr coatings using filtered cathodic vacuum arc depositions.

Substrate,	Inconel (Cr interlayer)
Pressure, Pa	4.0×10^{-3}
Arc current, A	65
Substrate voltage, V	−100
Coat/interval, sec	10/40

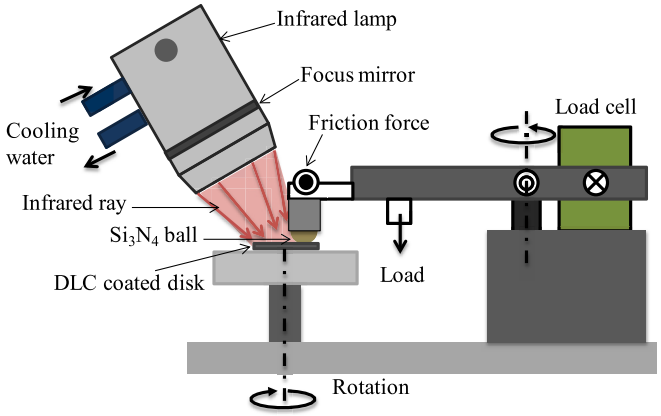

Fig. 2. Schematic diagram of ball on disk friction tester at high temperature, increasing temperature was employed by the infrared lamp; and the DLC-coated disk was held on the rotated stage, performing the friction between disk and held Si_3N_4 ball. The normal load was applied by the motionless weight, and the friction force was measured by a load cell.

deposition process. The pre arc process was employed to remove the water molecules and large particles adhered in the pipe duct. Argon-plasma was performed to remove the oxide layers and impurities on the surface of Inconel substrate, with 1.80 kV of discharge voltage and 16 sccm (standard cubic centimetre/min) of Argon flow rate. The main DLC deposition was conducted with an arc current of 80 A, as well as the substrate bias of −100 V. One deposition cycle consists of 10-second arc discharge, followed by a 40-second cooling interval. The details were listed in Table 1. During the deposition process the flow rate of Argon gas varied from 0 to 16 sccm for the a-C:B:$Cr_{0.5}$ coating as a preliminary exploration to optimize the deposition conditions, and 10 sccm was applied to other a-C:B:Cr coatings.

2.2. Structural characterization and surface observation of a-C:B:Cr coating

The coating thickness of doped-DLC was obtained by profilometer (Mitutoyo, SV-3100), measuring the step difference between coating and the marks prepared prior to the deposition. The nano-indentation with the 300 μN load (Elionix, ENT-1100a) was used to evaluate the hardness and Young's modulus, considering the thickness of doped-DLC, the indentation depth was controlled within the 1/10 of the DLC coatings to eliminate the influence from substrate. The Oliver & Pharr method was specifically utilized to extract the reduced Young's modulus, ensuring the reliability of the measured data.

The surface morphology of both ball and disk, as well the changes (worn area, debris and transfer layer) after friction test, were observed using a confocal laser scanning microscopy (Olympus, OLS5100, Japan). In addition, the scanning electron microscopy (SEM; Hitachi SU-8200, Japan) equipped with an energy-dispersive X-ray spectroscope (EDS; QUANTAX FlatQUAD) was also used to observe the frictional surface at the micrometer scale. EDS analysis was employed at a 5 keV of acceleration voltage to obtain the elemental mapping images and suspect the chemical composition of the bulk coating as well as the tribo-film.

Raman spectroscopy (Jasco, NRS-1000) with 532 nm laser was employed to analyze the structure of a-C:B:Cr coating and suspect the structure transition during the friction process. I_D/I_G ratio was used to evaluate the disorder and graphitization of carbonaceous material [25,62]. The collected Raman spectrum was deconvoluted into two-peaks (i.e., D and G peak) using Gaussian functions, and the intensity ratio of D and G peak, G peak position, as well as the full width at half maximum (FWHM) were respectively analyzed.

Chemical composition was estimated using the PHI Quantera III XPS instrument (ULVAC-PHI Inc., Japan), investigating the boron (B_{1s}) carbon (C_{1s}), oxide (O_{1s}) and chromium (Cr_{2p}) spectra. Each acquired narrow peak was deconvoluted to fit chemical bonds respectively, with background determined using the Shirley method; the calculated area ratio of fitting spectra in a narrow peak was used to compare the concentration of each chemical bonds [25].

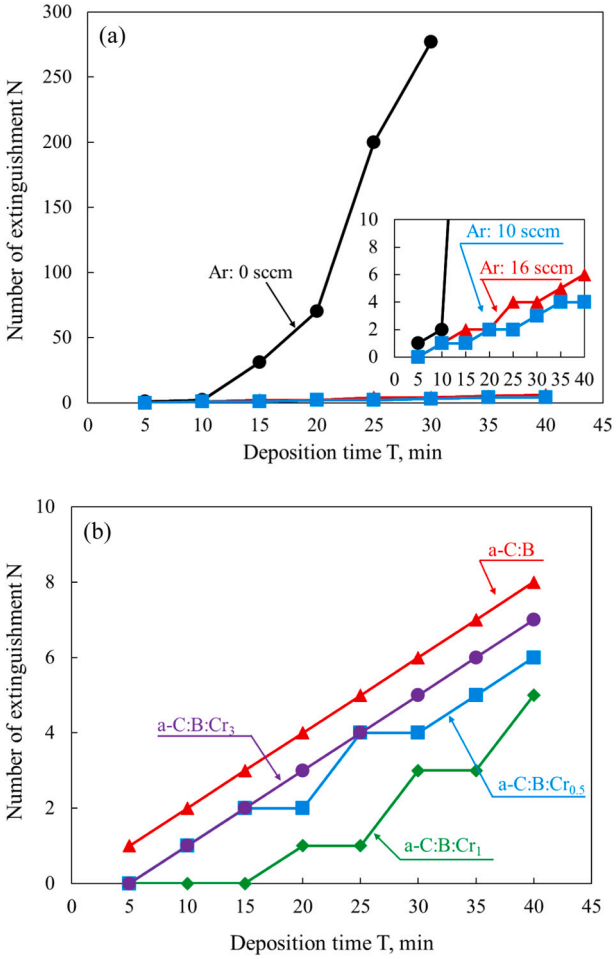

Fig. 3. Extinguishment numbers of arc discharge during the deposition of a-C:B:Cr coating demonstrated a dramatic suppression through introducing the Argon gas, as depicted in (a). However, excessive introduction of Argon gas led to a decrease in the deposition speed and hardness of a-C:B:Cr coating. Therefore, 10 sccm was selected as the optimal flow rate. (b) 10-sccm Argon gas can be perfectly applied to all kinds of a-C:B:Cr coating, with extinguishment numbers controlled below the 10 times within 40 min deposition for all cases.

2.3. Ball-on disk friction test at high temperature of 300 °C

The ball-on-disk friction tester was used to evaluate the tribological properties at 300 °C, as illustrated in Fig. 2. The a-C:B:Cr coating disk was held at the rotation stage, sliding against the Si_3N_4 ball (Ø = 8 mm) counterpart. The rotation speed was set as 200 rpm, and the diameter was 6 mm, corresponding to the sliding velocity of 62.8 mm/s. The normal load was applied to 1.0 N by the motionless weight. The specimens were heated by an infrared lamp in ambient air and maintained at the set temperature of 300 °C throughout the entire friction test. It took 45 min for the temperature to stabilize, after which the friction test was conducted for 5 mins (1000 cycles). The friction force was measured by a load cell and converted to the friction coefficient. To ensure the credibility, the friction tests were repeated for three times under the same conditions. The wear tracks of DLC disks and the wear scar of balls were observed using the confocal laser scanning microscopy; and the specific wear rate of DLC disks was calculated based on results measured

Table 2
The thickness and hardness of a-C:B:$Cr_{0.5}$ coating deposited under different flow rate of introduced Argon gas, were used as the selective parameters to determine optimal flow rate of Argon gas. It was found that 10 sccm Argon gas was able to deposit thicker and harder a-C:B:$Cr_{0.5}$ coating.

Flow rate of Argon gas, sccm	Thickness, nm	Hardness, GPa
0	20	9.2
10	110	12.4
16	72	9.8

by profilometer at the cross-sectional four points of the wear track.

3. Results

3.1. The suppression of arc discharge extinguishment with the introduction of Argon gas

Fig. 3 demonstrated the improvement effect on continuous coating with the introduction of Argon gas. We utilized the B/$Cr_{0.5}$-included carbon target to conduct a preliminary experiment, clarifying how the flow rate of Argon gas influenced the continuity of FCVA. We counted the extinguishment numbers to demonstrate the continuity of arc discharge. As shown in Fig. 3(a), without Argon gas being introduced, the extinguishment occurred as predicted. After a 10-minute coating, the extinguishment numbers exponentially increased, making the deposition of a-C:B:$Cr_{0.5}$ coating hardly conducted. Only 20 nm of a-C:B:$Cr_{0.5}$ coating was obtained after more than 40-minute deposition. Conversely, the extinguishment numbers dramatically decreased with the introduction of 10-sccm Argon gas, with only five-time extinguishment occurring within a 40-minute coating period. Furthermore, optimization of the flow rate of Argon gas was conducted. Introducing 16-sccm Argon gas under the same deposition condition resulted in a similar continuous deposition as the "10-sccm coating", with only three-time extinguishment, ensuring the normal deposition of element-doped DLC coating and repeatedly proving the effectiveness of Argon gas-assisted deposition. Herein, we selected the thickness and hardness of the DLC coating to estimate the efficiency of Argon gas-assisted deposition. As listed in the Table 2, under 40-minute deposition, the 10-sccm Argon gas assisted deposition could obtain the most optimized film, with thickness of 110 nm and hardness of 12.4 GPa. However, the 16-sccm Argon gas-assisted deposition only got a 72-nm film with the hardness of 9.8 GPa, suggesting that excessive introduction of Argon gas decreased the deposition rate. The reason for this will be discussed in the following content.

Based on the continuity, speed of deposition, and the hardness of a-C:B:Cr coating, the 10-sccm Argon gas-assisted deposition was selected as the main coating parameter in this study. As shown in Fig. 3(b), four types of boron-incorporated graphite with different chromium contents were used in this 10-sccm Argon gas-assisted deposition system. As expected, the extinguishment numbers were successfully suppressed within 10 occurrences during a 40-minute deposition period. Additionally, all a-C:B:Cr coatings achieved a thickness of over 100 nm. Specifically, the thicknesses of the four coatings were 225 nm (a-C:B), 128 nm (a-C:B:$Cr_{0.5}$), 142 nm (a-C:B:Cr_1), and 198 nm (a-C:B:Cr_3). Although the deposition speed of B/Cr co-incorporated graphite target was slightly decreased compared with the B-incorporated one, the variation in thickness among four coatings was within 100 nm. This range was considered to be within the same thin film region and was not expected to have a significant influence on the exploration of mechanical as well as the tribological properties. The effective deposition was believed to solve the conventional issue of element-included graphite target in the FCVA system, and more importantly, enrich the preparation methods of doped-DLC deposition.

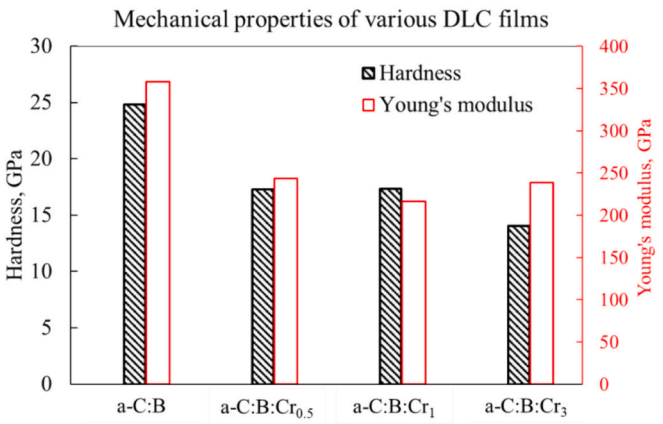

Fig. 4. The hardness and Young's modulus of three kinds of a-C:B:Cr coating.

Table 3
The I_D/I_G ratio, D peak and G peak, deconvoluted from Raman spectra of a-C:B:Cr coatings.

	a-C:B	a-C:B:$Cr_{0.5}$	a-C:B:Cr_1	a-C:B:Cr_3
I_D/I_G	0.36	0.63	0.73	1.49
D peak	1364	1374	1382	1384
G peak	1554	1553	1552	1550

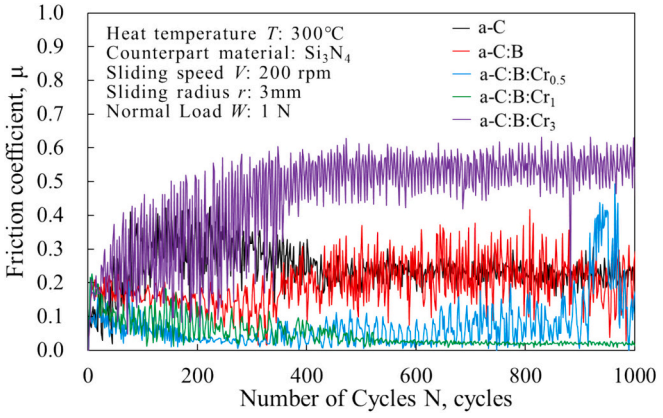

Fig. 5. Friction coefficient curve of a-C:B:Cr coating vs Si_3N_4 ball at 300 °C, all coatings exhibited a similar run-in period within the initial 400 cycles, and the friction coefficient of a-C:B:Cr_1 coating showed the smallest fluctuation during steady-state period, suggesting the stable tribo-film was formed between counterparts.

3.2. The mechanical properties of a-C:B:Cr coatings with various chromium elements concentration

The mechanical properties and structural characterization of four different a-C:B:Cr coatings were evaluated. As demonstrated in Fig. 4, the a-C:B coatings exhibited the highest hardness among the four coatings, with a value of 25 GPa. However, with the incorporation of Cr dopant, all three types of a-C:B:Cr coatings become softer, with hardness dropping to around 80 % of that of the a-C:B coating. This suggested that the incorporation of Cr dopant into-B-DLC lowered the mechanical properties of a-C:B:Cr coating.

Raman spectroscopy was utilized for the structural characterization, focusing on the conventional D peak and G peak of carbon-related materials and analyzing the influence caused by the incorporation of chromium dopant. The deconvoluted peak positions of the D peak and G peak were respectively listed in Table 3, and original I_D/I_G ratio clearly

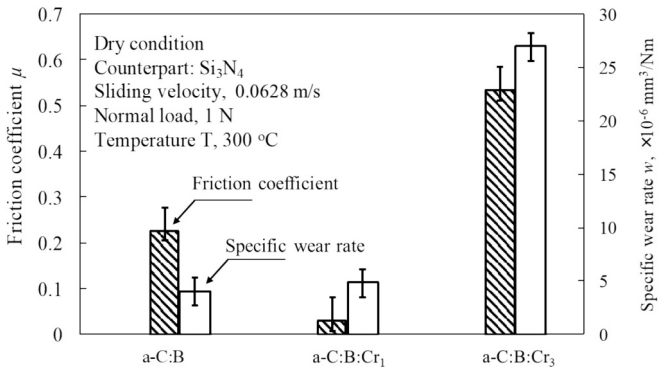

Fig. 6. The summary results of average friction coefficient and specific wear rate of a-C:B:Cr coating, a-C:B:Cr_1 coating exhibited the lowest friction coefficient of 0.02 and smaller specific wear rate of 5.0×10^{-6} mm^3/Nm; demonstrating that the incorporation of the optimal 1.0 at. % Cr-dopant improved the tribological properties of B-DLC.

demonstrated that with increasing content of Cr-dopant, the disorder structure of carbon atoms increased, and more graphite-like carbon has been formed.

3.3. Tribological properties of a-C:B:Cr coatings at high temperature of 300 °C

Since the initial evaluation on the B/Cr co-doped a-C coating has been conducted, the tribological properties were further estimated at a high temperature of 300 °C. Three groups of ball-on-disk friction tests were mainly conducted, using a-C:B coating, a-C:B:Cr_1 coating and a-C:B:Cr_3 coating. Additionally, the a-C coating and a-C:B:$Cr_{0.5}$ coating were included for basic discussion on friction coefficient as the reference group. The overall friction curve depicted in Fig. 5 suggested that the run-in period endured a short process of 400 cycles before entering the steady-state period.

The friction coefficient of a-C:B:Cr_1 coating has been decreasing since the initial run-in period, subsequently demonstrating stable low friction with minimal fluctuation since 500 cycles; and maintaining this state until the end of friction test. Conversely, the friction coefficient of a-C:B coating decreased during the run-in period, and gradually increased with a large fluctuation after 400 cycles. The a-C:B:Cr_3 coating exhibited the common behavior of increasing friction coefficient during the run-in period. After reaching the steady state, the increasing friction coefficient remained above 0.5. In addition, the a-C:B:$Cr_{0.5}$ showed the similar frictional behavior to a-C:B:Cr_1 coating, whereas with a higher friction coefficient and increasingly larger fluctuation after 350 cycles; the friction coefficient dramatically increased to 0.4 at the 900th cycle, and the black wear debris inside the wear track (shown in Fig. S2) indicated that the coating peeled off from the substrate. Therefore, the tribological properties of peeling-off a-C:B:$Cr_{0.5}$ coating would not be further explored in the following part. The a-C coating showed an increasing friction coefficient during run-in period, with friction coefficient staying at around 0.25 in the steady-state period.

The average friction coefficient at the steady-state period has been summarized in Fig. 6, along with the specific wear rate of each coating. The a-C:B:Cr_1 coating realized the lowest friction with the approximate value of 0.02, almost approaching the super low friction level. However, the a-C:B and a-C:B:Cr_3 coatings exhibited high friction coefficient of 0.22 and 0.53, respectively. Besides, both the a-C:B and a-C:B:Cr_1 coating showed the high wear resistance at the same level, where specific wear rates $<5.0 \times 10^{-6}$ mm^3/Nm, representing an 80 % reduction compared to the a-C:B:Cr_3 coating. Therefore, the a-C:B:Cr_1 coating has obtained the desired low friction and high wear resistance among the well-prepared a-C:B:Cr coatings.

4. Discussion

4.1. Effect of introducing Argon gas on arc discharge and deposition

When considering the strategy to suppress the extinguishment, it is essential to discuss the arc discharge process occurring on the surface of the graphite target. Typically, arc discharge was initially triggered on the surface of graphite target (cathode), giving rise to the cathode spot as a highly energetic emitting area. In these spots, graphite bulk material was melted and vaporized, leading to the ionization of carbon atoms due to collisions with accelerated electrons, thus generating carbon plasma. The extracted carbon plasma, under the influence of a magnetic field,

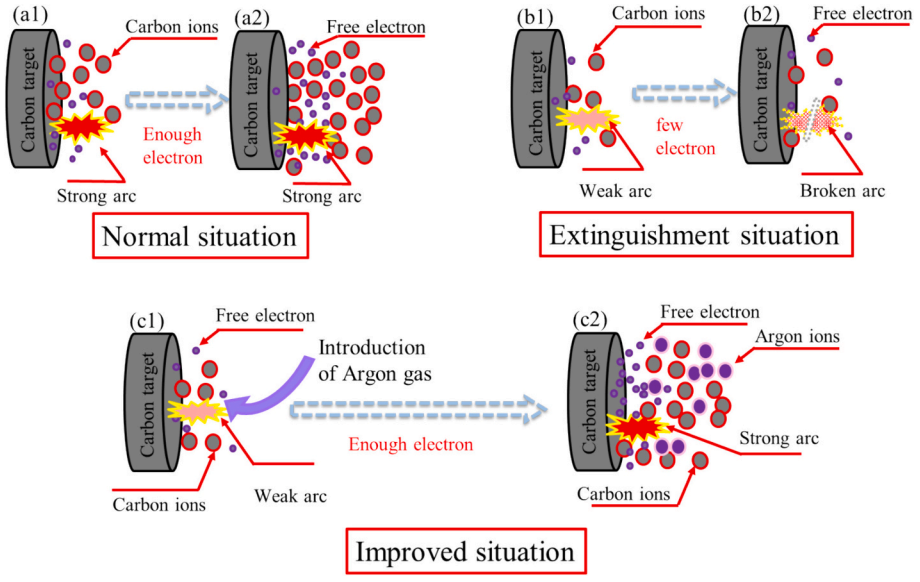

Fig. 7. Schematic diagram of effectiveness on continuous arc discharge through the introduction Argon gas. While using a dopant-included carbon target, the weak arc discharge might not generate enough free electron to sustain the subsequent arc discharge, resulting in a broken arc known as extinguishment. By introducing Argon gas into the carbon target, it participated in the arc discharge process and generated enough free electrons to strengthen the weak arc discharge, thereby solving the extinguishment issues.

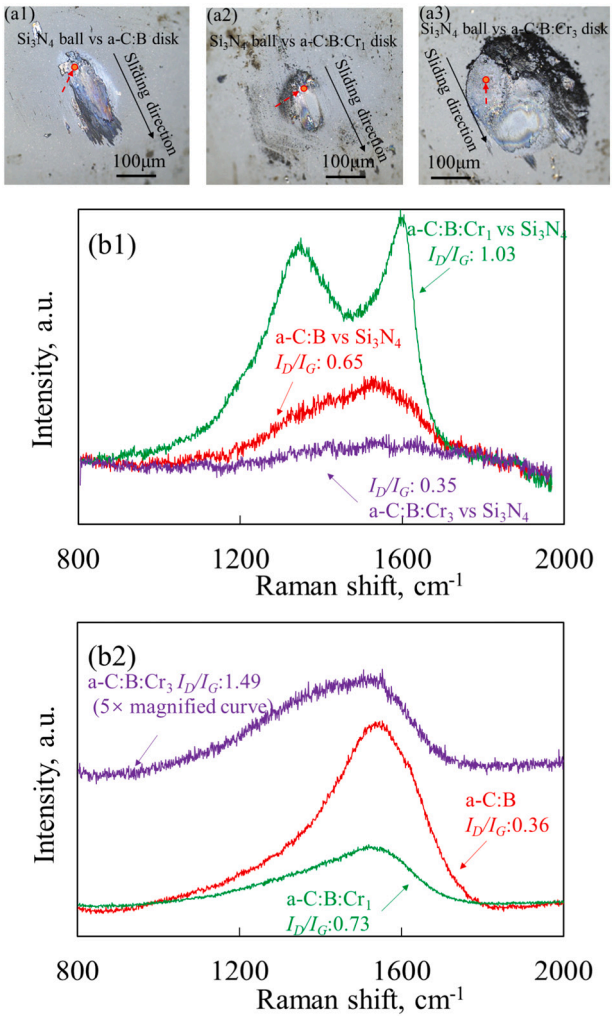

Fig. 8. Optical images of transfer layer on the Si_3N_4 ball surface, sliding against the (a1) a-C:B coating, (a2) a-C:B:Cr_1 coating, and (a3) a-C:B:Cr_3 coating. The transfer layer adhered on the Si_3N_4 ball surface was measured by Raman spectroscopy, with the Raman spectrum measured at the representative position (marked with red indicators) shown in (b1). The I_D/I_G ratio suggested that the graphite-like transfer layer of a-C:B:Cr_1 coating adhered on the surface of Si_3N_4 counterpart, resulting in stable ultra-low friction. The Raman spectrum of the as-deposited a-C:B:Cr coating was depicted in (b2). (For interpretation of the references to colour in this figure legend, the reader is referred to the web version of this article.)

was used for deposition. Simultaneously, the movement of certain electrons formed an electric path between anode and cathode, therefore, the electric potential promoted further arc discharge on the graphite cathode, which can be regarded as the driving force of maintaining continuous generation of plasma. In other words, plasma ignition occurred at the graphite cathode, where a sufficient number of free electrons were needed to sustain further arc discharge; as shown in Fig. 7 (a1) to (a2). Initially, in the original design of FCVA equipment, only the graphite target was used for DLC coating, where impact ionization (arc discharge) generated sufficient seed electrons to maintain continuous deposition. However, Paschen's law suggested that the material of the cathode influenced the creation of free electrons resulting from impacting ions. Therefore, incorporating other dopants into the graphite target reduced carbon plasma density, resulting in fewer free electrons available to maintain the electric path, as illustrated in Fig. 7(b1) to (b2). Consequently, the arc cannot be continuously discharged, becoming a significant reason for extinguishment. To address this issue, Argon gas was introduced to maintain continuous arc discharge in the FCVA system. Since Argon gas participated in the ionization process and released free electrons, the increasing free electrons built a stable electric path for the further arc discharge [63]. The schematic of this strategy was illustrated in Fig. 7(c1) to (c2). As described, the introduction of 10-sccm Argon gas notably reduced extinguishment numbers compared with the non-introduction of Argon gas assisted deposition. On the other hand, excessive introduction of Argon gas not only provided more free electrons, but also promoted the collision between Argon atoms and carbon ions. This decreased the mean free path of carbon plasma, reduced plasma energy and free electron, excitation and ultimately lowered plasma density. This might be the main factor leading to the significantly decreased deposition rate of 16-sccm Ar gas assisted coating.

4.2. *Surface characterization of friction counterparts and clarification on mechanism of low wear and friction of a-C:B:Cr_1 coating*

Generally, harder coating was considered to exhibit higher wear resistance, whereas in high-temperature atmosphere and under friction, structural transform could occur. Therefore, it became necessary to conduct more surface observation, as well as the structural characterization. Optical microscopy observations straightforwardly displayed the worn parts of coatings and their respective counterparts, pinpointing important areas for further surface analysis. As shown in Fig. 8(a), the average diameter of the wear scar on the Si_3N_4 ball sliding against the a-C:B and a-C:B:Cr_1 coating were within 100 μm, while that of a-C:B:Cr_3 coating was above 200 μm. Besides, transfer layers can be observed in the respective wear scars on the surface of Si_3N_4 ball; and the representative area within the transfer layer (marked by red circle) was

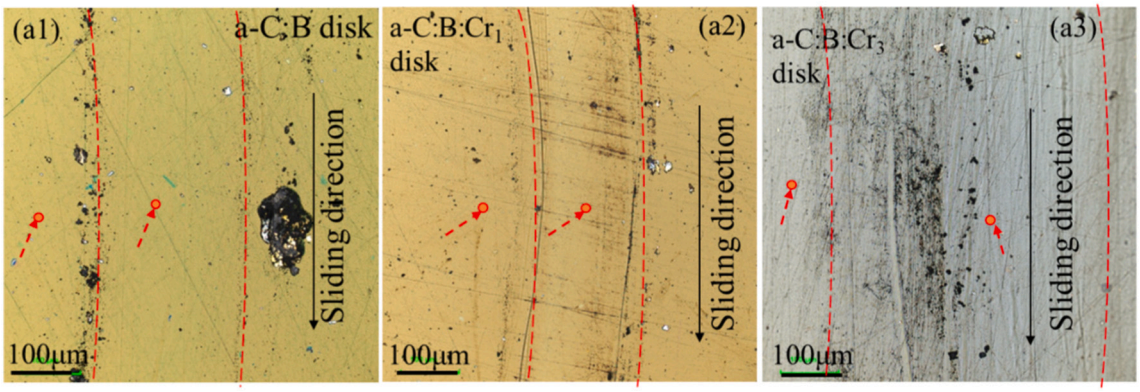

Fig. 9. Optical images of wear track of (a1) a-C:B coating, (a2) a-C:B:Cr_1 coating, and (a3) a-C:B:Cr_3 coating. The areas of "inside wear track" and "outside wear track" were respectively analyzed by XPS. The wear tracks of a-C:B and a-C:B:Cr_1 coatings appeared relatively clean and smooth, whereas the wear track of a-C:B:Cr_3 coating was predominantly covered with black wear debris (similar to oxidants, shown in Fig. S5-2(3)).

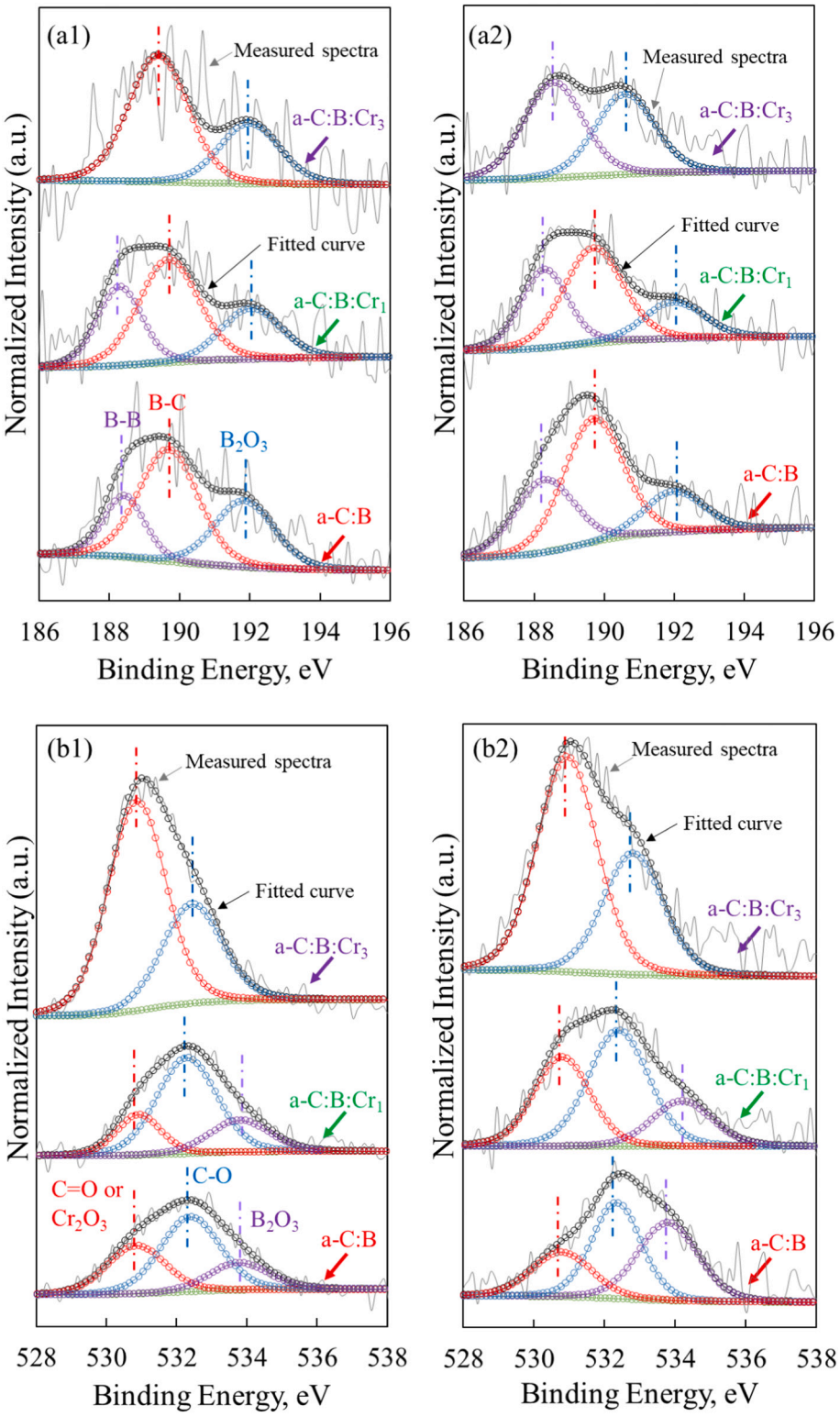

Fig. 10. B_{1s} spectra of a-C:B:Cr coatings, (a1) inside and (a2) outside the wear tracks. From the bottom to the top, the spectra was respectively a-C:B coating, a-C:B:Cr_1 coating, and a-C:B:Cr_3 coating. The O_{1s} spectra of a-C:B:Cr coatings, (b1) inside and (b2) outside the wear tracks. Again, from the bottom to the top, the spectra corresponded to a-C:B coating, a-C:B:Cr_1 coating, and a-C:B:Cr_3 coating.

measured by Raman spectroscopy. The spectra demonstrated in Fig. 8 (b1) indicated that the transfer layer from a-C:B:Cr_1 coating to the surface of Si_3N_4 ball (Fig. 8(a2)) exhibited a highest I_D/I_G ratio, with the value increased to 1.03 compared to as-deposited value of 0.73 (Fig. 8 (b2)). This suggested the graphitization process of amorphous DLC coating was largely accelerated and the transformed graphite-like carbon film was transferred to the surface of Si3N4 ball, thereby realizing the low friction between a-C:B:Cr_1 and Si_3N_4. A slightly transformed graphite-like carbon film with an I_D/I_G ratio of 0.65 (compared with the original 0.36 of the as-deposited a-C:B coating shown in Fig. 8(b2)) can

be detected on the surface of Si_3N_4 ball for the a-C:B coating group (Fig. 8(a1)), which might correspond to the products formed during the coefficient-decreasing process. These products have not maintained stable low friction, and the accumulated transferred wear debris of a-C:B coating took the lead, conversely resulting in the high friction. Furthermore, the a-C:B:Cr_3 coating group has not promoted the graphitization process, as evidenced by the low I_D/I_G ratio of 0.35 (Fig. 8(a3)), but also formed black materials on the surface of Si_3N_4 ball, indicating a strong oxidation process occurring during friction at the high temperature (Fig. S5).

Subsequently, the wear track of a-C:B:Cr coatings were also observed, as shown in Fig. 9. The width of each wear track was consistent with the diameter of the wear scar as discussed in Fig. 8(a1 to a3). Two deep scratches (Fig. S5-2) along the wear track of a-C:B:Cr_1 coating were clearly observed compared with the morphology of the other two wear tracks. Besides, the area outside the wear track of a-C:B:Cr_1 coating appeared clean, with minimal black wear debris at the side. In contrast, a significant amount of black wear debris was observed outside the wear track of the a-C:B coating. Furthermore, a large quantity of black wear debris appeared within the wear track of the a-C:B:Cr_3 coating, consistent with the black wear debris mentioned in the Fig. 8(a3). This suggested that the wear debris continuously existed between Si_3N_4 ball and a-C:B:Cr_3 disk as a third body, and the accumulation of more and more wear debris caused the high friction under high temperature conditions.

Moreover, the wear tracks of these three coatings were also characterized by XPS, and the representative areas (marked by the red circles) were shown in Fig. 10. Focusing on the B_{1s} spectra, we observed that the wear tracks of both a-C:B and a-C:B:Cr_1 coatings exhibited relatively stronger B_{1s} signals with less noise compared to the a-C:B:Cr_3 coating. Additionally, the presence of B—B bonds remained at a strong level for the a-C:B and a-C:B:Cr_1 coatings. However, in the case of the a-C:B:Cr_3 coating, the B—B bond was hardly detected, and it was predominantly transformed into C—B bonds. (the spectra comparison between inside (a1) and outside the wear track (a2)). These findings corresponded to the specific wear rates of the three coatings, suggesting a positive correlation between the presence of B—B bonds and wear resistance. The EDS results of both a-C:B and a-C:B:Cr_1 coatings (depicted in Fig. S5-1 and S5-2) revealed the concentration of each element. Specifically, the boron element maintained a stable level of 20 % both inside and outside the wear track, while oxygen accounted for a concentration lower than 2 %. These findings indicated that the incorporation of boron effectively suppressed the oxidation reaction under the conditions of high temperatures and friction tests.

The analysis of the O_{1s} spectra provided further insight into the superior wear resistance of the a-C:B and a-C:B:Cr_1 coatings. When comparing the spectra inside and outside the wear track, it was observed that the C=O/Cr_2O_3 bonds were transformed into C—O bonds in both coatings. Conversely, in the case of the a-C:B:Cr_3 coatings, a large proportion of C=O/Cr_2O_3 bonds was evident both inside and outside the wear track. These findings suggested that excessive incorporation of Cr dopant promoted the formation of Cr_2O_3, which was considered an adverse third body leading to severe wear. In addition, the existence of B_2O_3 were detected both inside and outside the wear track of a-C:B and a-C:B:Cr_1 coatings, whereas B_2O_3 peak was hardly obtained towards the a-C:B:Cr_3 coatings. These results suggested B_2O_3 would exhibit the beneficial effect on wear resistance. Furthermore, B dopant was proved to lead to the superior wear resistance. Moreover, Cr-dopant did not exhibit a direct contribution on the superior wear properties, whereas a stable formation of graphite-like transfer layer only occurred in the case of the a-C:B:Cr_1 and its counterparts; suggesting that the importance of Cr-dopant on improving the tribological properties of B-DLC, as well as the necessity of appropriate concentration during deposition.

5. Conclusion

This research addressed the development of B/Cr co-doped DLC and the improvement of its tribological properties at high temperature of 300 °C. We investigated the Argon gas assisted deposition process in the FCVA system to suppress the arc extinguishment issue and elucidate the mechanism of Argon gas assisted deposition. The optimal flow rate of 10 sccm was found to be suitable for all four types of a-C:B:Cr coatings with different Cr-dopant concentration (0, 0.5, 1.0 and 3.0 at. %). Subsequently, we studied the tribological properties of various Cr-containing a-C:B coatings and found that the a-C:B:Cr_1 coating exhibited the super low friction with an approximate friction coefficient of 0.02 and lowest specific wear rate of $<5.0 \times 10^{-6}$ mm^3/Nm. Raman spectroscopy revealed that the formation of a stable graphite-like transfer layer on the surface of Si_3N_4 balls (counterpart) might be cause of low friction, the XPS results clarified that the incorporation of boron into DLC coating improved the wear resistance at high temperature, possibly due to the presence of rich B—B bond. Furthermore, although Cr-dopant did not exhibit direct effect on improvement of wear properties, the proper dopant concentration was proved to be an essential factor in the formation of a stable graphite-like transfer layer, leading to super low friction.

CRediT authorship contribution statement

Ruixi Zhang: Writing – original draft, Methodology, Investigation. **Woo-Young Lee:** Writing – review & editing, Methodology, Investigation. **Noritsugu Umehara:** Writing – review & editing, Supervision, Resources, Project administration, Conceptualization. **Takayuki Tokoroyama:** Writing – review & editing, Supervision, Methodology, Investigation. **Motoyuki Murashima:** Writing – review & editing, Methodology. **Yuji Takimoto:** Writing – review & editing, Resources, Methodology.

Declaration of competing interest

The authors declare that they have no known competing financial interests or personal relationship that could appeared to influence the work reported in this paper.

Data availability statement

The data used in this research is available upon request.

Appendix A. Supplementary data

Supplementary data to this article can be found online at https://doi.org/10.1016/j.surfcoat.2024.130968.

References

[1] R. Hauert, An overview on the tribological behavior of diamond-like carbon in technical and medical applications, Tribol. Int. 37 (2004) 991–1003, https://doi.org/10.1016/j.triboint.2004.07.017.
[2] P. Písařík, M. Jelínek, K. Smetana, B. Dvořánková, T. Kocourek, J. Zemek, D. Chvostová, Study of optical properties and biocompatibility of DLC films characterized by sp3 bonds, Appl. Phys. A Mater. Sci. Process. 112 (2013) 143–148, https://doi.org/10.1007/s00339-012-7216-8.
[3] J. Barriga, M. Kalin, K. Van Acker, K. Vercammen, A. Ortega, L. Leiaristi, Tribological performance of titanium doped and pure DLC coatings combined with a synthetic bio-lubricant, Wear 261 (2006) 9–14, https://doi.org/10.1016/j.wear.2005.09.004.
[4] M. Jelinek, A. Voss, T. Kocourek, M. Mozafari, V. Vymětalová, M. Zezulová, P. Písařík, A. Kotzianová, C. Popov, J. Mikšovský, Comparison of the surface properties of DLC and ultrananocrystalline diamond films with respect to their bio-applications, Physica Status Solidi (A) Applications and Materials Science 210 (2013) 2106–2110, https://doi.org/10.1002/pssa.201228713.
[5] R. Hauert, A review of modified DLC coatings for biological applications, Diam. Relat. Mater. 12 (2003) 583–589, https://doi.org/10.1016/S0925-9635(03)00081-5.

[6] S. Miyake, T. Shindo, M. Miyake, Regression analysis of the effect of bias voltage on nano- and macrotribological properties of diamond-like carbon films deposited by a filtered cathodic vacuum arc ion-plating method, J. Nanomater. 2014 (2014), https://doi.org/10.1155/2014/657619.
[7] Y. Fujii, T. Imai, Y. Miyamoto, N. Ueda, M. Hosoo, T. Harigai, Y. Suda, H. Takikawa, H. Tanoue, M. Kamiya, M. Taki, Y. Hasegawa, N. Tsuji, S. Kaneko, Dry machining of metal using an engraving cutter coated with a droplet-free ta-C film prepared via a T-shape filtered arc deposition, Surf. Coat. Technol. 307 (2016) 1029–1033, https://doi.org/10.1016/j.surfcoat.2016.07.037.
[8] M. Pandey, D. Bhatacharyya, D.S. Patil, K. Ramachandran, N. Venkatramani, A. K. Dua, Structural and optical properties of diamond like carbon films, J. Alloys Compd. 386 (2005) 296–302, https://doi.org/10.1016/j.jallcom.2004.05.067.
[9] B. Pandey, P.P. Pal, S. Bera, S.K. Ray, A.K. Kar, Effect of nickel incorporation on microstructural and optical properties of electrodeposited diamond like carbon (DLC) thin films, Appl. Surf. Sci. 261 (2012) 789–799, https://doi.org/10.1016/j.apsusc.2012.08.101.
[10] A. Grill, Electrical and optical properties of diamond-like carbon, Thin Solid Films 355–356 (1999) 189–193, https://doi.org/10.1016/S0040-6090(99)00516-7.
[11] M. Hiratsuka, H. Nakamori, Y. Kogo, M. Sakurai, N. Ohtake, H. Saitoh, Correlation between optical properties and hardness of diamond-like carbon films, Journal of Solid Mechanics and Materials Engineering 7 (2013) 187–198, https://doi.org/10.1299/jmmp.7.187.
[12] M. Jarratt, J. Stallard, N.M. Renevier, D.G. Teer, An improved diamond-like carbon coating with exceptional wear properties, Diam. Relat. Mater. 12 (2003) 1003–1007, https://doi.org/10.1016/S0925-9635(02)00296-0.
[13] P. Xu, Y. Wang, X. Cao, X. Nie, W. Yue, G. Zhang, The tribological properties of DLC/SiC and DLC/Si3N4 under different relative humidity: the transition from abrasive wear to tribo-chemical reaction, Ceram. Int. 47 (2021) 3901–3910, https://doi.org/10.1016/j.ceramint.2020.09.252.
[14] A. Erdemir, C. Donnet, Tribology of diamond-like carbon films: recent progress and future prospects, J. Phys. D. Appl. Phys. 39 (2006), https://doi.org/10.1088/0022-3727/39/18/R01.
[15] L. Cao, J. Liu, Y. Wan, J. Pu, Corrosion and tribocorrosion behavior of W doped DLC coating in artificial seawater, Diam. Relat. Mater. 109 (2020), https://doi.org/10.1016/j.diamond.2020.108019.
[16] D. Martinez-Martinez, J.T.M. De Hosson, On the deposition and properties of DLC protective coatings on elastomers: a critical review, Surf. Coat. Technol. 258 (2014) 677–690, https://doi.org/10.1016/j.surfcoat.2014.08.016.
[17] Y.J. Jang, G.T. Kim, Y.J. Kang, D.S. Kim, J.K. Kim, A study on thick coatings of tetrahedral amorphous carbon deposited by filtered cathode vacuum arc plasma, in: J Mater Res, Cambridge University Press, 2016, pp. 1957–1963, https://doi.org/10.1557/jmr.2016.78.
[18] Y.C. Ean, Y.J. Jang, J.K. Kim, W.L. Yun Hsien, N.J. Siambun, S.S. Kim, Effect of substrate bias on the tribological behavior of ta-C coating prepared by filtered cathodic vacuum arc, Int. J. Precis. Eng. Manuf. 18 (2017) 779–784, https://doi.org/10.1007/s12541-017-0093-5.
[19] Y. Shibata, T. Kimura, S. Nakao, K. Azuma, Preparation of silicon-doped diamond-like carbon films with electrical conductivity by reactive high-power impulse magnetron sputtering combined with a plasma-based ion implantation system, Diam. Relat. Mater. 101 (2020), https://doi.org/10.1016/j.diamond.2019.107635.
[20] W.Y. Lee, T. Tokoroyama, Y.J. Jang, N. Umehara, Effect of substrate bias and temperature on friction and wear properties for ta-C coating prepared under different substrate bias voltages with filtered cathodic vacuum arc deposition, Tribology Online 13 (2018) 241–247, https://doi.org/10.2474/trol.13.241.
[21] W.-Y. Lee, T. Tokoroyama, M. Murashima, N. Umehara, Investigating running-in behavior to understand wear behavior of ta-C coating with filtered cathodic vacuum arc deposition, Jurnal Tribologi 23 (2019) (2019) 38–47.
[22] W. Dai, P. Ke, A. Wang, Microstructure and property evolution of Cr-DLC films with different Cr content deposited by a hybrid beam technique, Vacuum 85 (2011) 792–797, https://doi.org/10.1016/j.vacuum.2010.11.013.
[23] I.C. Müller, J. Sharp, W.M. Rainforth, P. Hovsepian, A. Ehiasarian, Tribological response and characterization of Mo–W doped DLC coating, Wear 376–377 (2017) 1622–1629, https://doi.org/10.1016/j.wear.2016.11.036.
[24] M. Haji Ghasemi, B. Ghasemi, H.R. Mohamadian Semnani, M. Erfanmanesh, A comparative study of duty cycle and argon/methane flow ratio effect on the tribological behavior of DLC coatings over nitrided Astaloy Mo-based steel, Ceram. Int. 47 (2021) 12467–12475, https://doi.org/10.1016/j.ceramint.2021.01.104.
[25] E.C.T. Ba, M.R. Dumont, P.S. Martins, B. da Silva Pinheiro, M.P.M. da Cruz, J. W. Barbosa, Deconvolution process approach in Raman spectra of DLC coating to determine the sp3 hybridization content using the ID/IG ratio in relation to the quantification determined by X-ray photoelectron spectroscopy, Diam. Relat. Mater. 122 (2022), https://doi.org/10.1016/j.diamond.2021.108818.
[26] M. Muhyiddin, B. Mustafa, N. Umehara, T. Tokoroyama, M. Murashima, A. Shibata, Y. Utsumi, H. Moriguchi, Effect of pillar and mesh structure of tetrahedral amorphous carbon (ta-C) coatings on the wear properties and fracture toughness of the coating, Tribol. Online 14 (5) (2019) 388–397, https://doi.org/10.2474/trol.14.388.
[27] M.M. Bin Mustafa, N. Umehara, T. Tokoroyama, M. Murashima, A. Shibata, Y. Utsumi, H. Moriguchi, Effect of mesh structure of tetrahedral amorphous carbon (ta-C) coating on friction and wear properties under base-oil lubrication condition, Tribol. Int. 147 (2020), https://doi.org/10.1016/j.triboint.2019.01.016.
[28] X. Deng, H. Kousaka, T. Tokoroyama, N. Umehara, Deposition and tribological behaviors of ternary BCN coatings at elevated temperatures, Surf. Coat. Technol. 259 (2014) 2–6, https://doi.org/10.1016/j.surfcoat.2014.08.087.
[29] Y. Tokuta, M. Kawaguchi, A. Shimizu, S. Sasaki, Effects of pre-heat treatment on tribological properties of DLC film, Tribol. Lett. 49 (2013) 341–349, https://doi.org/10.1007/s11249-012-0073-y.
[30] E.L. Dalibón, L. Escalada, S. Simison, C. Forsich, D. Heim, S.P. Brühl, Mechanical and corrosion behavior of thick and soft DLC coatings, Surf. Coat. Technol. 312 (2017) 101–109, https://doi.org/10.1016/j.surfcoat.2016.10.006.
[31] M. Evaristo, F. Fernandes, A. Cavaleiro, Room and high temperature tribological behaviour of W-DLC coatings produced by DCMS and hybrid DCMS-HiPIMS configuration, Coatings 10 (2020), https://doi.org/10.3390/coatings10040319.
[32] T. Ohana, T. Nakamura, M. Suzuki, A. Tanaka, Y. Koga, Tribological properties and characterization of DLC films deposited by pulsed bias CVD, Diam. Relat. Mater. 13 (2004) 1500–1504, https://doi.org/10.1016/j.diamond.2003.11.019.
[33] W. Dai, H. Zheng, G. Wu, A. Wang, Effect of bias voltage on growth property of Cr-DLC film prepared by linear ion beam deposition technique, Vacuum 85 (2010) 231–235, https://doi.org/10.1016/j.vacuum.2010.06.001.
[34] D. Bootkul, B. Supsermpol, N. Saenphinit, C. Aramwit, S. Intarasiri, Nitrogen doping for adhesion improvement of DLC film deposited on Si substrate by Filtered Cathodic Vacuum Arc (FCVA) technique, Appl. Surf. Sci. 310 (2014) 284–292, https://doi.org/10.1016/j.apsusc.2014.03.059.
[35] H. Takikawa, K. Izumi, R. Miyano, T. Sakakibara, DLC thin film preparation by cathodic arc deposition with a super droplet-free system, Surf. Coat. Technol. 163–164 (2003) 368–373, https://doi.org/10.1016/S0257-8972(02)00629-1.
[36] N. Miyakawa, S. Minamisawa, H. Takikawa, T. Sakakibara, Physical-chemical hybrid deposition of DLC film on rubber by T-shape filtered-arc-deposition, in: Vacuum, 2004, pp. 611–617, https://doi.org/10.1016/j.vacuum.2003.12.079.
[37] H. Takikawa, N. Miyakawa, S. Minamisawa, T. Sakakibara, Fabrication of diamond-like carbon film on rubber by T-shape filtered-arc-deposition under the influence of various ambient gases, Thin Solid Films (2004) 143–150, https://doi.org/10.1016/j.tsf.2003.12.029.
[38] M. Kamiya, H. Tanoue, H. Takikawa, M. Taki, Y. Hasegawa, M. Kumagai, Preparation of various DLC films by T-shaped filtered arc deposition and the effect of heat treatment on film properties, Vacuum 83 (2008) 510–514, https://doi.org/10.1016/j.vacuum.2008.04.016.
[39] H. Cao, X. Ye, H. Li, F. Qi, Q. Wang, X. Ouyang, N. Zhao, B. Liao, Microstructure, mechanical and tribological properties of multilayer Ti-DLC thick films on Al alloys by filtered cathodic vacuum arc technology, Mater. Des. 198 (2021), https://doi.org/10.1016/j.matdes.2020.109320.
[40] W.Y. Lee, Y.J. Jang, T. Tokoroyama, M. Murashima, N. Umehara, Effect of defects on wear behavior in ta-C coating prepared by filtered cathodic vacuum arc deposition, Diam. Relat. Mater. 105 (2020), https://doi.org/10.1016/j.diamond.2020.107789.
[41] A. Grill, V. Patel, B.S. Meyerson, Temperature and Bias Effects on the Physical and Tribological Properties of Diamond-like Carbon, 1991.
[42] H. Liu', A. Tanaka, K. Umeda, The Tribological Characteristics of Diamond-like Carbon Films at Elevated Temperatures, 1999.
[43] X. Deng, H. Kousaka, T. Tokoroyama, N. Umehara, Thermal stability and high-temperature tribological properties of a-C:H and Si-DLC deposited by microwave sheath voltage combination plasma, Tribology Online 8 (2013) 257–264, https://doi.org/10.2474/trol.8.257.
[44] S. Bhowmick, M. Lou, M.Z.U. Khan, A. Banerji, A.T. Alpas, Role of an oxygen atmosphere in high temperature sliding behaviour of W containing diamond-like carbon (W-DLC), Surf. Coat. Technol. 332 (2017) 399–407, https://doi.org/10.1016/j.surfcoat.2017.06.093.
[45] Q. Zeng, O. Eryilmaz, A. Erdemir, Superlubricity of the DLC films-related friction system at elevated temperature, RSC Adv. 5 (2015) 93147–93154, https://doi.org/10.1039/c5ra16084g.
[46] Q. Zeng, Z. Ning, High-temperature tribological properties of diamond-like carbon films: a review, Rev. Adv. Mater. Sci. 60 (2021) 276–292, https://doi.org/10.1515/rams-2021-0028.
[47] S. Bhowmick, S. Shirzadian, A.T. Alpas, High-temperature tribological behavior of Ti containing diamond-like carbon coatings with emphasis on running-in coefficient of friction, Surf. Coat. Technol. 431 (2022), https://doi.org/10.1016/j.surfcoat.2021.127995.
[48] X. Deng, H. Kousaka, T. Tokoroyama, N. Umehara, Tribological behavior of tetrahedral amorphous carbon (ta-C) coatings at elevated temperatures, Tribol. Int. 75 (2014) 98–103, https://doi.org/10.1016/j.triboint.2014.04.002.
[49] D. Hofmann, S. Kunkel, K. Bewilogua, R. Wittorf, From DLC to Si-DLC based layer systems with optimized properties for tribological applications, Surf. Coat. Technol. 215 (2013) 357–363, https://doi.org/10.1016/j.surfcoat.2012.06.094.
[50] C.W. Zou, H.J. Wang, L. Feng, S.W. Xue, Effects of Cr concentrations on the microstructure, hardness, and temperature-dependent tribological properties of Cr-DLC coatings, Appl. Surf. Sci. 286 (2013) 137–141, https://doi.org/10.1016/j.apsusc.2013.09.036.
[51] A. Banerji, S. Bhowmick, A.T. Alpas, High temperature tribological behavior of W containing diamond-like carbon (DLC) coating against titanium alloys, Surf. Coat. Technol. 241 (2014) 93–104, https://doi.org/10.1016/j.surfcoat.2013.10.075.
[52] K. Nemoto, N. Umehara, T. Tokoroyama, M. Murashima, Y. Takimoto, K. Nakamichi, Deposition of ta-C:B coating by FCVA using boron doped target and its tribological behaviors at elevated temperature up to 300°C, Journal of Japanese Society of Tribologists 63 (10) (2018) 699–705, https://doi.org/10.18914/tribologist.18-00003.
[53] W. Yu, J. Wang, W. Huang, L. Cui, L. Wang, Improving high temperature tribological performances of Si doped diamond-like carbon by using W interlayer, Tribol. Int. 146 (2020), https://doi.org/10.1016/j.triboint.2020.106241.
[54] O. Jantschner, S.K. Field, D. Music, V.L. Terziyska, J.M. Schneider, F. Munnik, K. Zorn, C. Mitterer, Sputtered Si-containing low-friction carbon coatings for

elevated temperatures, Tribol. Int. 77 (2014) 15–23, https://doi.org/10.1016/j.triboint.2014.04.006.
[55] T. Vuchkov, T. Bin Yaqub, A. Cavaleiro, The influence of the deposition pressure on the composition and the mechanical properties of W–S–C coatings deposited by magnetron sputtering in semi-industrial conditions, Vacuum 184 (2021), https://doi.org/10.1016/j.vacuum.2020.109963.
[56] M. Bai, L. Yang, J. Li, L. Luo, S. Sun, B. Inkson, Mechanical and tribological properties of Si and W doped diamond like carbon (DLC) under dry reciprocating sliding conditions, Wear 484–485 (2021), https://doi.org/10.1016/j.wear.2021.204046.
[57] J. Peng, Y. Xiao, M. Yang, J. Liao, Effect of nitrogen doping on the microstructure and thermal stability of diamond-like carbon coatings containing silicon and oxygen, Surf. Coat. Technol. 421 (2021), https://doi.org/10.1016/j.surfcoat.2021.127479.
[58] B.J. Rodriguez, T.L. Schiller, D. Proprentner, M. Walker, C.T.J. Low, B. Shollock, H. Sun, P. Navabpour, Effect of chromium doping on high temperature tribological properties of silicon-doped diamond-like carbon films, Tribol. Int. 152 (2020), https://doi.org/10.1016/j.triboint.2020.106546.
[59] J.A. Santiago, I. Fernández-Martínez, J.C. Sánchez-López, T.C. Rojas, A. Wennberg, V. Bellido-González, J.M. Molina-Aldareguia, M.A. Monclús, R. González-Arrabal, Tribomechanical properties of hard Cr-doped DLC coatings deposited by low-frequency HiPIMS, Surf. Coat. Technol. 382 (2020), https://doi.org/10.1016/j.surfcoat.2019.124899.
[60] X. Liu, R. Yamaguchi, N. Umehara, M. Murashima, T. Tokoroyama, Effect of oil temperature and counterpart material on the wear mechanism of ta-CNx coating under base oil lubrication, Wear 390–391 (2017) 312–321, https://doi.org/10.1016/j.wear.2017.08.012.
[61] X. Liu, N. Umehara, T. Tokoroyama, M. Murashima, Tribological properties of ta-CNx coating sliding against steel and sapphire in unlubricated condition, Tribol. Int. 131 (2019) 102–111, https://doi.org/10.1016/j.triboint.2018.10.022.
[62] R. Arenal, A.C. Ferrari, S. Reich, L. Wirtz, J.Y. Mevellec, S. Lefrant, A. Rubio, A. Loiseau, Raman spectroscopy of single-wall boron nitride nanotubes, Nano Lett. 6 (2006) 1812–1816, https://doi.org/10.1021/nl0602544.
[63] H. Tanoue, M. Kamiya, S. Oke, Y. Suda, H. Takikawa, Y. Hasegawa, M. Taki, M. Kumagai, M. Kano, T. Ishikawa, H. Yasui, Argon-dominated plasma beam generated by filtered vacuum arc and its substrate etching, Appl. Surf. Sci. 255 (2009) 7780–7785, https://doi.org/10.1016/j.apsusc.2009.04.170.